Thermal stability and miscibility of co-evaporated methyl ammonium lead halide ($MAPbX_3$, X=I,Br,Cl) thin films analysed by *in situ* X-ray diffraction

Paul Pistor,[a,*] Thomas Burwig,[a] Carlo Brzuska,[a] Björn Weber,[b] and Wolfgang Fränzel[a]

[a.] *Martin-Luther-Universität Halle-Wittenberg, Institute of Physics, Von-Danckelmann-Platz 3, 06120 Halle (Saale), Germany*
[b.] *Martin-Luther-Universität Halle-Wittenberg, Institute of Chemistry, Von-Danckelmann-Platz 3, 06120 Halle (Saale), Germany*
**Corresponding author:* paul.pistor@physik.uni-halle.de

Abstract

We present the identification of crystalline phases by *in situ* X-ray diffraction during growth and monitor the phase evolution during subsequent thermal treatment of $CH_3NH_3PbX_3$ (X=I,Br,Cl) perovskite thin films. Thin films are prepared by vacuum-based two-source co-evaporation using various methyl ammonium (MA) halide and lead halide (PbX_2) precursors. The single halide perovskite materials $MAPbI_3$, $MAPbBr_3$ and $MAPbCl_3$ are prepared without secondary phases and an upper thermal limit for the decomposition into the corresponding lead halides is established. We show that at a substrate temperature of 120°C, the halide in $MAPbI_3$/$MAPbBr_3$ thin films can be completely and reversibly exchanged upon exposure to the opposite MA halide. We monitor the temporal evolution of the conversion process *in situ* and discuss differences in the forward- and backward conversion. For the deposition of mixed $MAPb(I,Br)_3$ perovskite thin films, different growth routes are suggested and evaluted in terms of growth with single phases or phase segregations. Our results are discussed in a broader context considering the I/Br miscibility. Finally we propose a new growth route for the synthesizis of single phase mixed $MAPb(I_{1-x}Br_x)_3$ thin films in the range from x = 0.3 to 1 by two source co-evaporation and discuss the implication of our results.

Introduction

Hybrid organic-inorganic lead halide perovskites for solar cells

Research on photovoltaic (PV) energy conversion has been shaken in the last years by the appearance of a new class of absorber materials called perovskites. These new hybrid organic-inorganic compounds where first explored as light harvesters in 2009[1] and gained exponentially increasing interest during the last five years since their first successful application in thin film solar cells with efficiencies exceeding 10% in 2012.[2, 3] Currently, best cell efficiencies have well surpassed 20%,[4, 5] putting them on the same performance level as the best conventional polycrystalline PV technologies such as polycrystalline Si, $Cu(In,Ga)Se_2$ or CdTe.

Remarkable optoelectronic properties such as strong photoluminescence and long charge carrier diffusion lengths (> 1 μm),[6, 7] the possibility to apply simple and cheap non-vacuum-based deposition techniques (e.g. spin coating) and a tuneable band gap suitable for both, single junction and tandem applications have further boosted scientific and industrial interest. While the race to highest efficiency solar cells was extremely fast and successful, reports about the intrinsic instability of the hybrid halide perovskite materials when exposed to moderate levels of heat,[8, 9] moisture[10] and even light[11, 12] currently put an obstacle to industrial considerations.[13-15] This also severely limits the reproducibility of results, especially because many of the fundamental properties have been reported for wet-chemical processes which depend critically on air exposure times, ambient conditions, surface conditioning and quality of solvents, precursors and substrates. It is therefore not an easy task to derive more general conclusions about this material class and there is still a strong need for further fundamental characterisation under very well defined conditions.

Wet-chemical methodologies such as spin-coating allow very fast progress and high sampling rates on a laboratory scale and have up to now been applied in the grand majority of publications. However, we believe that vacuum-based technologies such as co-evaporation should not be ignored, as they allow a precise parameter control, better reproducibility and fast processing on very large areas, which makes them attractive under a large-scale industrial point of view. Several groups have already successfully deposited $MAPbI_3$ thin film by two source co-evaporation[16, 17] yielding working solar cells with efficiencies of up to 15%.[18, 19] The two-source co-evaporation allowed to grow dense planar films with large crystals, where the thickness variations were much smaller as compared to solution-coated films[18]. Additional intrinsic advantages of the co-evaporation technique over solution-based preparation are the ability to grow films with arbitrary thickness and the avoidance of toxic solvents. We follow this approach and report

here on our progress in understanding the fundamental phase formation and decomposition mechanisms of perovskite thin films synthesized by co-evaporation of MAX and PbX_2 (X=I,Br,Cl) precursors investigated in situ by X-ray diffraction (XRD).

It is well known and has been extensively reported that $MAPI_3$ decomposes easily under thermal stress and/or exposure to air/humidity.[14, 20, 21] However, the rate of decomposition and the degree of instability is not well established and seems to be strongly related to the deposition pathway. More information on the intrinsic thermal stability of $MAPbX_3$ is therefore desirable. Furthermore, air exposure times of grown films between synthesis and measurement (and relative humidity levels) are crucial for all decomposition analysis and are unfortunately usually not detailed. It is clear that if thin films had ever been exposed to air/humidity prior to any stability analysis, some moisture is likely to have soaked into the films. This will lead to a slow decomposition during a long time even if effective air exposure times have been kept short and the actual stability analysis afterwards is carried out in dry conditions. We find it therefore important to note that in contrast to most *ex situ* measurements, films in our experiments have not been exposed to air or humidity at any point during the investigation, which enables us to explore the fundamental thermal stability of unexposed perovskite films.

The prototype of the perovskite absorber material applied in solar cells is based on organic-inorganic methyl ammonium lead iodine ($MAPbI_3$). The most common variations and combinations of constituents are substitution of methyl ammonium (MA) by formamidinium (FA) or Cs or a (partial) substitution of the iodine by Br or Cl. $MAPbI_3$ has a band gap of 1.51 eV,[22] suitable for single-junction photovoltaic applications. Following the line I-Br-Cl, the ionic radius decreases, the Pb-X bond strength increases[23] and consequently the band gap of the material is also increased (see table 1). The analogous perovskite with bromine, $MAPbBr_3$, has a band gap of 2.42 eV,[24] which is suitable for light emitting diodes, but in principle too high for efficient solar energy harvesting. $MAPbCl_3$ shows an even higher band gap of 3.16 eV.

A clear advantage of hybrid lead halides is the possibility to tune the bandgap by intermixing some of the perovskite components. As for the mixed halide $MAPbX_3$ perovskites, there is consensus that the $MAPbBr_3$-$MAPbCl_3$ system is completely miscible,[25-27] while the $MAPbI_3$-$MAPbCl_3$ is not because the difference of the atomic radii is too large.[26, 28] The mixed $MAPb(I,Br)_3$ system allows band gaps interesting for tandem solar cell applications but the miscibility is still under debate.[29] While Bolink and co-workers have reported a sequential evaporation-conversion process,[30] up to our knowledge the deposition of mixed $MAPb(I,Br)_3$ thin films by co-evaporation from two sources has not been reported so far.

In our contribution we explore the possibility to control the growth of single phase perovskite thin films by two-source co-evaporation under high vacuum conditions. We focus on the most widely used methyl ammonium lead halide perovskites ($MAPbX_3$) with X= I, Br, and Cl. Firstly, we will investigate the growth mechanisms of the single halide perovskites and introduce the working principle and potential of our specialized *in situ* X-ray diffraction (XRD) setup. We continue studying in detail the behaviour of the grown $MAPbX_3$ thin films under thermal stress and monitor their decomposition routes.

We will then concentrate on the mixed $MAPb(I,Br)_3$ system, which is the most relevant one for photovoltaic applications. Here, we first investigate *in situ* the exchange of the halide anions in grown films and the conversion of $MAPbI_3$ into $MAPbBr_3$ and vice versa. Finally, the potential of different growth routes to prepare mixed $MAPb(I,Br)_3$ thin films in static two-source co-evaporation will be evaluated and the best growth route to obtain single phase material is identified.

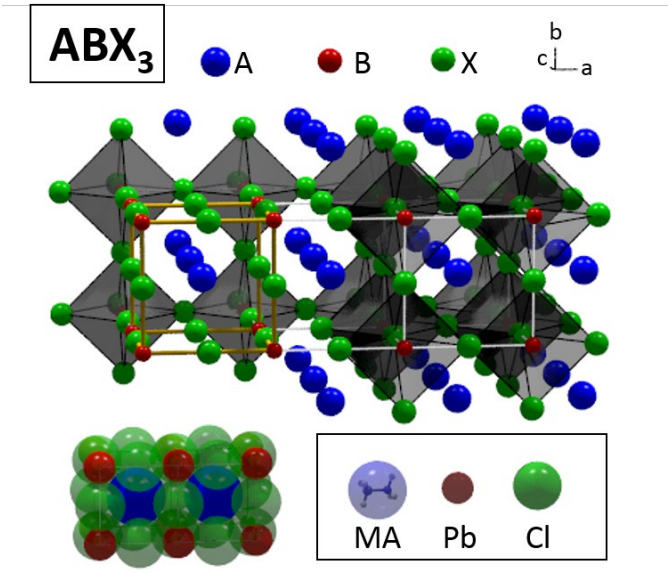

Figure 1: *Above: Sketch of the perovskite crystal structure for materials with sum formula ABX_3. Note that in this presentation the atoms are displayed smaller than corresponding to their atomic radii for better visualization. Below: Presentation of $MAPbCl_3$ with properly scaled atomic radii.*

Crystal structure of methyl ammonium lead halides ($MAPbX_3$, X=I,Br,Cl)

The ideal cubic crystal structure with space group Pm3m (No. 221) and sum formula ABX_3 is the aristotype for the group of materials called perovskite.[22] A sketch of the crystal structure is depicted in figure 1. In these materials, a large cation A is located at the Wyckoff position 1a coordinated to 12 X anions (position 3c). The position of the large cation A can be occupied by a large ion such as Ca or Cs, but also by small molecules such as methyl ammonium (MA) or formamidinium (FA) as in $MAPbX_3$. B is usually a smaller metal (position 1c) which is bonded to six X anions forming a dense framework of corner sharing octahedra. The larger A cations are located in the voids between these octahedra. The A, B cations and the X anions can come with different atomic radii R_A, R_B, and R_X which predict the stability of a perovskite according to the Goldschmidt equation[31]:

$$t = \frac{(R_A + R_X)}{\sqrt{2}(R_B + R_X)}.$$

Here *t* is the tolerance factor which should lie between 0.9 and 1 for the ideal cubic structure. A non-ideal proportion of the A, B, X atomic radii results in a distortion of the ideal cubic crystal structure where the B-X octahedra get tilted and form hettotypes with lower symmetry.[32] Usually, the high temperature α-phase of perovskites crystallizes in the ideal cubic structure, as is the case for the three lead halide perovskites $MAPbI_3$, $MAPbBr_3$ and $MAPbCl_3$. Upon cooling, they undergo subsequent phase transitions towards one or several tetragonal β- and orthorhombic γ–phases with lowered symmetry. These polymorphs differentiate in the tilting and rotating of the PbX_6 octahedra.[22, 33, 34]

The crystal structure and phase transitions of $MAPbX_3$ perovskites have been studied extensively.[22, 35, 36] At 343 K, $MAPbI_3$ has the ideal cubic perovskite structure with space group Pm3m and lattice parameters a=6.276 Å.[22] The transition from the high temperature cubic α-phase to the tetragonal β-phase with space group *I4/mcm* takes place at 327-330 K,[22] followed by a transition towards the orthorhombic γ-$MAPbI_3$ with space group *Pnma* at approximately 162 K. Similar transitions are observed for $MAPbBr_3$ and $MAPbCl_3$. $MAPbBr_3$ has a cubic crystal structure at room temperature (a=5,901 Å)[36] and transforms into a tetragonal structure below 236.6 K.[35] Two different tetragonal configurations are reported for this compound and an orthorhombic γ-configuration is found for temperatures below 148.8 K. For $MAPbCl_3$, two different orthorhombic configurations have been found at low temperatures.[37] The transition temperatures of the cubic $MAPbX_3$ perovskites (X=I,Br,Cl) is listed together with other important crystallographic data in table 1. Here, the **Table 2:** Comparison of crystallographic properties of $MAPbI_3$, $MAPbBr_3$ and $MAPbCl_3$ perovskites. The lattice parameter *a* is given for $MAPbBr_3$ and $MAPbCl_3$ at room temperature and for $MAPbI_3$ at 70°C.Goldschmidt tolerance factors have been calculated with ionic radii provided by Shannon for the inorganic ions (Pb: 1.19 Å)[38] and an estimated effective radius of 2.17 Å for the protonated methyl ammonium $[CH_3NH_3]^+$ as introduced by Kieslich and co-workers.[32] From the transition temperatures it is clear that at room temperature only $MAPbI_3$ adopts a tetragonal crystal structure, while the other two compounds are already in the high temperature cubic α-phase. An indicative of the decomposition temperature as determined and described later on in this manuscript is added to a schematic representation of the phase transitions in figure 6.

Experimental *in situ* XRD monitoring and thin film co-evaporation setup

The growth of $MAPbX_3$ (X=I,Br,Cl) by co-evaporation in vacuum can be achieved by evaporating the corresponding methyl ammonium halides (MAX) and the lead halide (PbX_2) simultaneously. We will in the following show that the synthesis of thin films with this method is straight forward and use it as an example to introduce the capability to monitor thin films *in situ* by X-ray diffraction with the setup installed in our co-evaporation chamber. The chamber is usually operated at a base pressure of $2*10^{-5}$ mbar. The MAX crucible temperature is set in the temperature range between 110°C and 130°C, while the PbX_2 evaporation sources are operated at slightly higher temperatures (PbI_2: 300°C; $PbBr_2$: 300°C: $PbCl_2$: 350°C). During MAX evaporation, the chamber pressure usually increases to values around $(5.0\text{-}10.0)*10^{-4}$ mbar. If not stated otherwise, during the growth of perovskite $MAPbX_3$ thin films, the substrate is made of standard soda-lime glass and is not actively heated. Thin film thickness can be monitored by the interferences of scattered laser light signals (650 nm and 1550 nm) and a quartz microbalance. If not stated otherwise, thin films in the following experiments had thicknesses between 500 and 700 nm. An entrance and exit window placed at opposing sides of the chamber allows the X-ray beam to enter and leave the chamber. These windows are freshly covered with Kapton tape before each process. The X-ray system is operated with a Cu Kα source at a fixed incident angle and a position-sensitive X-ray detector covering an angular 2Θ-range of approximately 12°-40°. Counts within one scan are usually recorded over 60s. XRD peak position and peak areas have been fitted with the analysis software PDX-L after background subtraction using a pseudo-Voigt profile. More details on the in situ XRD setup can be found in references (39, 40).

Table 1: Comparison of crystallographic properties of $MAPbI_3$, $MAPbBr_3$ and $MAPbCl_3$ perovskites. The lattice parameter *a* is given for $MAPbBr_3$ and $MAPbCl_3$ at room temperature and for $MAPbI_3$ at 70°C.

$MAPbX_3$	X=I	X=Br	X=Cl
Ionic radius of halide [38]	2.20 Å	1.96 Å	1.82 Å
Tolerance factor *t*	0.91	0.93	0.94
Band gap [22, 24]	1.51 eV	2.42 eV	3.16 eV
Cubic high temperature α-phase			
Space group	Pm3m	Pm3m	Pm3m
Lattice parameter *a* [22, 36]	6.276 Å	5.901 Å	5.675 Å
Transition temperature [22, 35]	330K	237K	178K

Monitoring the growth and decomposition of $MAPbX_3$ thin films with *in situ* XRD

Monitoring the growth of $MAPbX_3$ (X=I,Br,Cl) thin films

Figure 2 summarizes the data accumulated during the subsequent growth of three different single halide $MAPbX_3$ thin

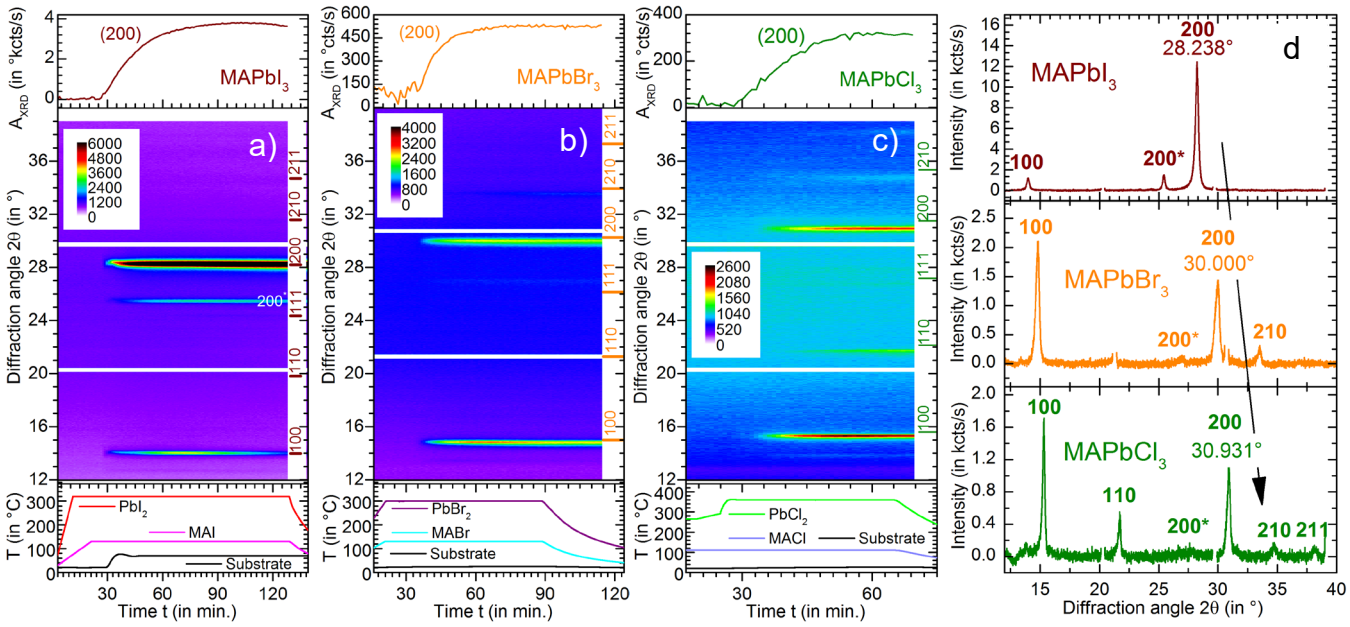

Figure 2: Growth of single halide **a)** $MAPbI_3$, **b)** $MAPbBr_3$ and **c)** $MAPbCl_3$ thin films by two-source co-evaporation. Each graph displays the evolution over time of the main process parameters such as the crucible and substrate temperature (below), a color-coded representation of the in situ XRD data collected during the deposition process (middle graph) and the evolution of the integrated peak area of (200) Bragg peak of the cubic $MAPbX_3$ perovskite phase. d) Comparison of single XRD scans recorded at the end of each deposition process.

films. In figure 2 a), the growth of a $MAPbI_3$ thin film is presented. In these compact representations, in the lower part of the graph, information about the growth process is depicted. In this case, the temporal evolution of the PbI_2/MAI crucible and the substrate temperatures during the growth are plotted. While during the other growth processes the substrate is usually not heated, in this case the substrate temperature was set to 70°C, because we wanted grow $MAPbI_3$ also in the cubic phase for better comparison. In the middle part, we present how the X-ray diffraction evolves over time (from left to right on the X-axis). Each row corresponds to an XRD measurement over the angular range from 12° to 40° (from bottom to top on the y-axis). In these maps, the intensity of the X-ray diffraction is represented by a colour code. On the right hand side of this colour map, brown bars indicate the position of the main XRD peaks of cubic $MAPbI_3$ from literature.[22] After an initial heating phase of approximately 20-25 minutes, the PbI_2 shutter is opened and $MAPbI_3$ starts to grow. The (200) peak is observed with very high intensity, while other prominent peaks as for example the (110) or (210) are missing. This means that our film grows in a pronounced preferential orientation. The detection of the (100) peak is also supressed under this preferential orientation due the fixed incident angle with static source-detector positions in these scans. Because of the very high intensity of the (200) peak, even the contribution from the Cu Kβ line can be observed at 25.47° and is marked in the picture with 200*. In the upper part, selected data extracted from the XRD analysis are plotted. As an example, in figures 2 a)-c) we have plotted the integrated peak area of the most intense (200) peak as a function of time. Here, the increasing thin film thickness is reflected in an increasing intensity of the XRD contributions.

Similar graphs are obtained for the growth of $MAPbBr_3$ and $MAPbCl_3$, which are displayed in figures 2 b) and c), demonstrating that the growth of $MAPbX_3$ thin films by co-evaporation is in fact straight forward. Although these films are also preferentially orientated to some extent, other peaks in addition to the (100) and (200) can still be observed with low intensities. The XRD analysis shows that the three single halide $MAPbX_3$ thin films grow in a single phase and no contributions from MAX or PbX_2 secondary phases can be observed. All three films grow in a cubic perovskite crystal structure with decreasing lattice parameters from I to Br to Cl. This translates into a shift of the position of the (200) peak to higher diffraction angles (MAPbI3: 28.24°, $MAPbBr_3$: 30.00°, $MAPbCl_3$: 30.93°), in agreement with expectation and literature. The final XRD measurement for the three depositions can be compared in figure 2 d).

Thermal decomposition of $MAPbX_3$ thin films in vacuum

After proving the possibility to grow single halide perovskites by simple co-evaporation we are interested in comparing the thermal stability of the grown films. For this purpose, the grown films were heated without vacuum break inside the chamber with a linear temperature ramp of 3 K/s. During the complete heating sequence, the evolution of phases was monitored with *in situ* XRD.

The results are depicted in figure 3. The lower graph shows how the substrate temperature increases linearly with time. In figure 3 a) we can clearly observe how the characteristic peaks of $MAPbI_3$ start to slowly loose intensity for temperatures above 150°C, before they completely vanish at temperatures above 250°C. Instead, new peaks arise above 200°C, which can be easily identified as PbI_2 (see also the bars at the left side of the

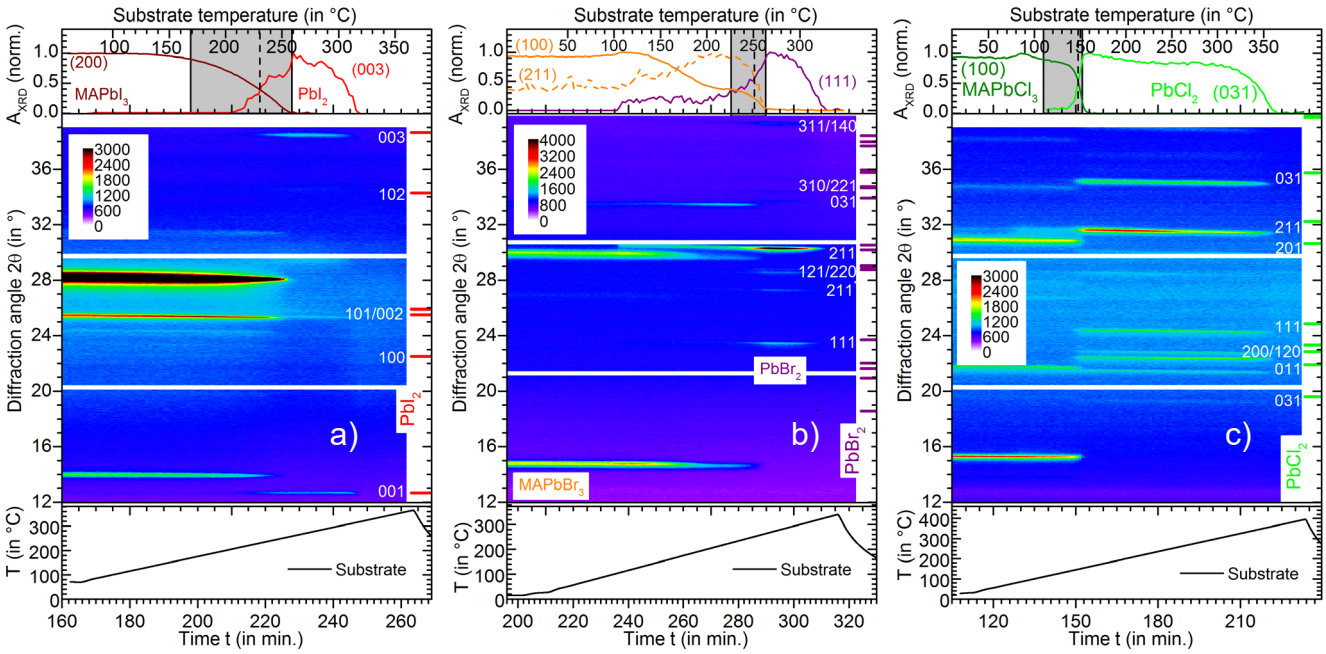

Figure 3: Heating and decomposition of the three single halide $MAPbX_3$ thin films represented in figure 2. The lower graph shows the ramping of the substrate temperature. In the middle graph, a color-coded representation of the in situ XRD data collected during the annealing process is depicted. The upper graph shows the evolution of the normalized integrated peak intensity of the representative Bragg peaks of the observed phases. **a)** $MAPbI_3$, **b)** $MAPbBr_3$, **c)** $MAPbCl_3$.

colour map). Above 320°C, the PbI_2 also sublimes and its characteristic XRD peaks vanish. In the upper part, the evolution of the normalised integrated peak area A_{XRD} of the $MAPI_3$ (200) and PbI2 (003) peak are displayed. The exact onset of decomposition cannot be determined from this simple experiment in a categorical manner. Nevertheless, for this comparative study we have deliberately elected and marked three points in the graphs: I) The point where A_{XRD} ($MAPbI_3$) is diminished to 90% of its maximum value, II) the point where the normalized A_{XRD} ($MAPbI_3$) = A_{XRD} (PbI_2) and the point where A_{XRD} (PbI_2) has reached 90% of its maximum value. In the following discussions, we will treat these three points as indicators for I) the onset of $MAPbX_3$ decomposition, II) the critical temperature T_c where approximately half of the $MAPbX_3$ is decomposed and III) the point where nearly all $MAPbX_3$ has been turned into the lead halide. These points are represented in the upper graph by the beginning (I) and end (III) of a shaded area and a dashed line (II).

Similar to $MAPbI_3$, the $MAPbBr_3$ thin film shows loss of MABr and decomposition into $PbBr_2$ upon heating (Fig. 3 b). However, before decomposing, the preferential orientation in the (200) direction is reduced in favor of a (211) orientation. Similar effects on orientation have also been previously observed for $MAPbI_3$ films.[39] This induces additional changes in the $MAPbX_3$ peak intensities which complicate the interpretation, but it seems that the decomposition of $MAPbBr_3$ thin films occur at slightly higher temperatures compared to $MAPbI_3$. This is clearly not the case for $MAPbCl_3$, which shows a very sharp change from $MAPbCl_3$ to $PbCl_2$ already at temperatures as low as 150°C (figure 3 c)). In conclusion, all three perovskite films show the same decomposition pathway at slightly different temperatures (150-250°C). First, the organic MAX evaporates from the film leaving the pure lead halide behind. In our experiments with a linear temperature ramp of 3 K/min. approximately half of the perovskite film is decomposed at the critical temperature T_c of 230°C ($MAPbI_3$), 251°C ($MAPbBr_3$) and 148°C ($MAPbCl_3$). At still higher temperatures, the lead halide also evaporates, leaving a blank glass substrate behind after the process. In the following paragraphs, we will continue with an investigation of the mixed MAPb(I,Br) system.

Halide exchange

I. $MAPbI_3$ -> $MAPbBr_3$

Several groups have reported about the possibility to easily exchange the halide in methylammonium lead halide perovskites.[41-43] We follow this line and will first try to convert $MAPbI_3$ into $MAPbBr_3$ inside the evaporation chamber. Theoretical calculations of Brivio et al. predict a miscibility gap of the $MAPbI_3$ – $MAPbBr_3$ system. The width of this miscibility gap however decreases with increasing temperature and at the critical temperature of 70°C the gap should be closed and both compound should intermix completely.[44] According to this, at a substrate temperature of 120°C the two perovskite structures $MAPbI_3$ and $MAPbBr_3$ should be completely miscible.

In order to investigate this, we first deposit a $MAPbI_3$ thin film by co-evaporating MAI and PbI_2 the same way as described previously (Fig. 4 a). After a single phase $MAPbI_3$ perovskite thin film with thickness of approximately 510 nm is grown, the $PbBr_2$ shutter is closed and the MABr and $PbBr_2$ sources are cooled down (t_1). Subsequently, the evaporation of MABr is started. In order to facilitate the halide exchange, the substrate is then heated to 120°C (t_2). In consequence, the hot $MAPbI_3$ thin films are now exposed to a constant flux of MABr molecules.

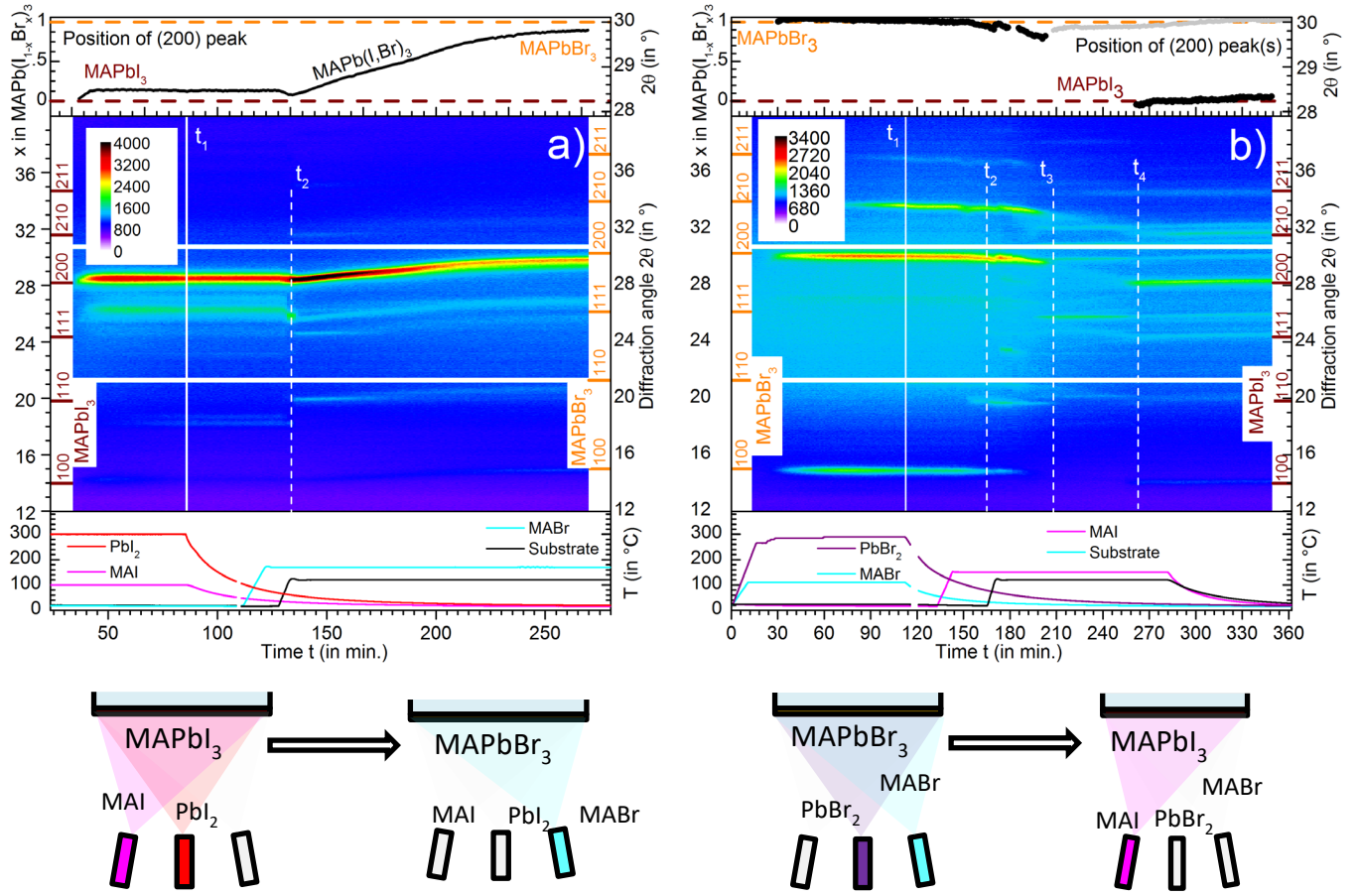

Figure 4: a) Growth of a $MAPbI_3$ thin film by two source co-evaporation and subsequent conversion into $MAPbBr_3$ upon exposure to MABr at a substrate temperature of 120°C. **b)** Growth of a $MAPbBr_3$ thin film and subsequent conversion into $MAPbI_3$. The top graph of both figures shows the evolution of the (200) peak position during the course of the experiment.

Upon heating and exposure to MABr, the initial $MAPbI_3$ (200) peak gains intensity and then starts shifting continuously towards higher diffraction angles. Assuming Vegard´s law,[45] the lattice parameter of $MAPb(I,Br)_3$ should vary linearly with composition between the two single halide perovskites. The position of the (200) peak can therefore be directly translated into a Br/(I+Br) ratio x of the mixed compound $MAPb(I_{1-x}Br_x)_3$. In the upper part of the diagram in figure 4 a), we have plotted the peak position of the (200) peak extracted from a fit to the XRD data. The peak positions of the two pure single halide perovskites are marked in this diagram with two dotted lines (brown: $MAPbI_3$ at 28.238° and orange: $MAPbBr_3$ at 30.000°). At the left hand side, the peak position is related to the I/Br ratio assuming Vegard´s law.

After a continuous shift to higher diffraction angles, the $MAPb(I,Br)_3$ (200) peak position finally levels off at 29.80(2)°. This is only slightly below the peak position measured for the pure $MAPbBr_3$ (30.00°). As the higher substrate temperature already accounts for a small thermal shift of 0.16° to lower diffraction angles, we conclude that after the halide exchange the film is completely converted into $MAPbBr_3$. In this case, the conversion took place through a gradual exchange of the I by Br, without distorting the crystal structure. This means that the perovskite film underwent the complete compositional range from pure $MAPbI_3$ to $MAPbBr_3$ while maintaining and preserving the high crystallinity and ordering of the crystal lattice at all times, in agreement with the prediction of Brivio and co-workers.

These observations are in contrast to the following experiment, where the halide exchange is induced the other way around, starting with a single halide $MAPbBr_3$ perovskite.

II. $MAPbBr_3$ -> $MAPbI_3$

Figure 4 b) shows the conversion of a $MAPbBr_3$ perovskite film into a $MAPbI_3$ thin film upon exposure to MAI. The experiment is conducted in the same way as the last one, except that we start with the co-evaporation of MABr/$PbBr_2$ to grow a $MAPbBr_3$ thin film first (590 nm), and then heat the substrate and expose the grown film to a flux of MAI. Figure 4 b) shows clearly how from time t_2 on, the main peaks of the $MAPbBr_3$ perovskite start shifting to lower diffraction angles. However, and in contrast to the last experiment, at the same time their intensity is strongly reduced. Both, thermal expansion and the exchange of Br ions by I ions will cause a lattice expansion explaining the shift to lower diffraction angles. At time t_3, the main (200) peak has nearly vanished. Only a small broad band with a maximum at 29.83(3)° remains. The position of this residual peak stays constant and only gradually shifts to higher diffraction angles again when the sample is cooled down at the end of the experiment, finishing at 30.03(3)° and at less than

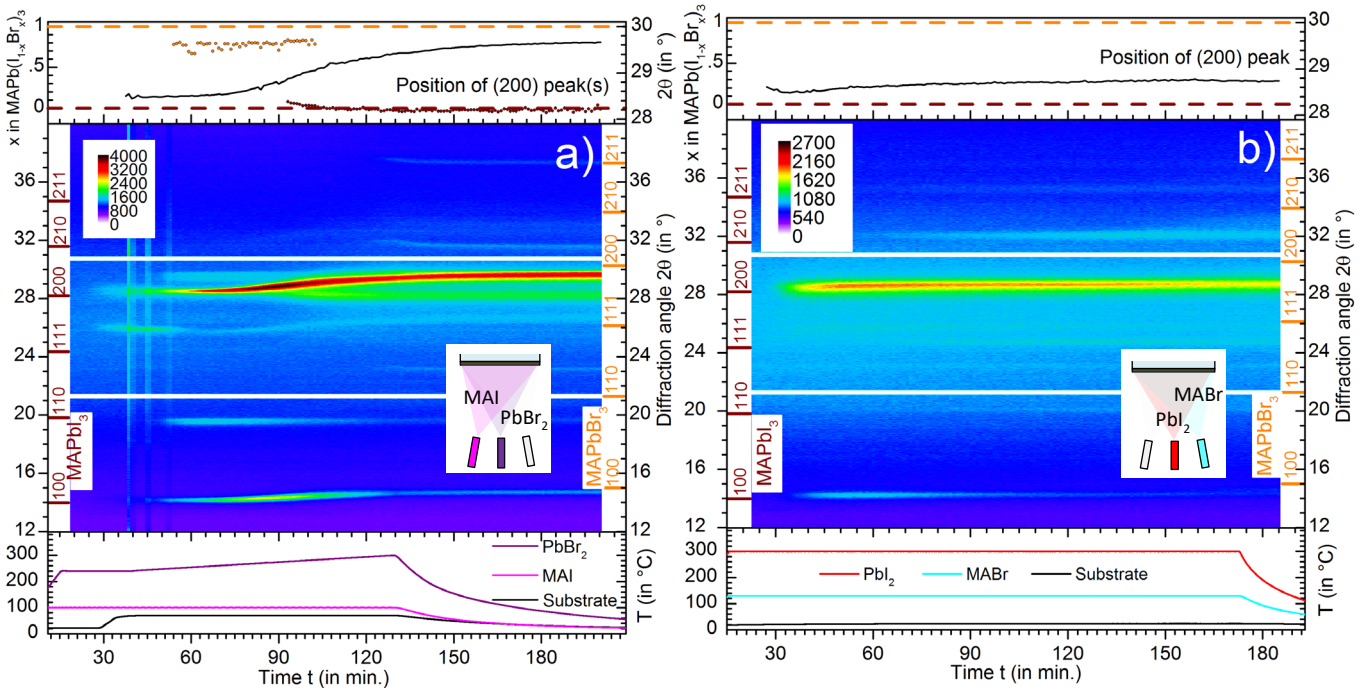

Figure 5: Growth of mixed $MAPb(I,Br)_3$ thin films by two-source co-evaporation. **a)** Co-evaporation of MAI and $PbBr_2$. Please note the increasing $PbBr_2$ substrate temperature resulting in an increasing $PbBr_2$ flux towards the substrate during the course of the experiment. b) Static growth of single phase $MAPbI_2Br$ thin films by co-evaporation of MABr and PbI_2.

12 % of its maximum intensity. Also around time t_3 a new peak arises at approximately 25.8°, which is assigned to the 111 peak of $MAPbBr_3$. This change in the peak intensity of different $MAPbBr_3$ peaks is again interpreted as a change in the preferential orientation of the $MAPbBr_3$ thin film, similar to the changing preferential orientation observed for the $MAPbBr_3$ thin film in figure 3 b). At time t_4, a new peak arises at 28.17(3)° and becomes soon the most intense peak. This peak appears simultaneously with other peaks characteristic for the $MAPbI_3$ perovskite. At the end of the experiment, the remaining XRD peaks correspond to the single halide $MAPbI_3$, with small residues of the initial $MAPbBr_3$.

In summary, we were indeed able in this experiment to nearly completely exchange the Br in $MAPbBr_3$ and substitute it with I. However, the exchange was not based on a continuous exchange of halides as in the former experiment. To the contrary, our results indicate that the crystal structure of the initial perovskite over time got severely distorted and then build up its crystalline structure again upon incorporation of the I ions. This is not predicted by the theoretical calculations of Brivio et al., in fact a similar behaviour would rather be expected if a fundamental miscibility gap between the two compounds existed.

We conclude with a simple remark: it is much easier in terms of the crystal lattice to replace I by Br, than the other way around. The implication of this will be discussed further in the discussion section. Please note that during equivalent experiments with unheated substrates, we did not observe any halide exchange during the timescale of our experiments (1-3 hours).

Growing mixed $MAPb(I,Br)_3$ thin films by two source co-evaporation

I. Co-evaporation of MAI and $PbBr_2$

In the next step, we try to grow mixed MAPb(I,Br) thin films by co-evaporating MAI and $PbBr_2$, in analogy to the initial work on co-evaporated $MAPb(I,Cl)_3$ thin films, where MAI and $PbCl_2$ were used as precursors.[18, 28] Since a relation between the $MAI/PbBr_2$ flux ratio and the amount of I/Br inside the deposited final $MAPb(I,Br)_3$ thin film is to be expected, several different depositions with varying $PbBr_2$ fluxes at constant MAI evaporation rates have been realized. Figure 5 a) summarizes the outcomes of these experiments in an illustrative manner. At the beginning, a low $PbBr_2$ crucible temperature leads to a small flux of $PbBr_2$ molecules arriving at the substrate and therefore a huge excess of MAI. A thin film with perovskite crystal structure forms. The position of the (200) peak is 28.48(2)°, very close to the pure $MAPbI_3$ perovskite. We then start to increase the $PbBr_2$ flux arriving at the substrate by linearly increasing the $PbBr_2$ source temperature.

Two observations can be made: 1) A new peak close to the position of the $MAPbBr_3$ (200) peak appears. 2) The (200) peak is split into two peaks, with the most intense contribution gradually shifting to higher diffraction angles and the second contribution shifting only slightly to lower angles. The first contribution eventually approaches 29.66° and merges with the new peak at high diffraction angles observed in 1). The second contribution stays nearly constant and only slightly shifts to lower diffraction angles, finishing at 28.24(2)°. In consequence, for a short intermediate time, even three separate peaks can be distinguished in the range between 28° and 30°. We interpret the observed phenomena in the following way: 1) A new, very Br-rich $MAPb(I,Br)_3$ thin film starts growing on top of the deposited very I-rich $MAPb(I,Br)_3$ at the beginning, 2) gradually some additional Br is incorporated into the growing film, while

some of the initially grown I-rich $MAPb(I,Br)_3$ is preserved. Over the course of the experiment, the most intense (200) peak gradually shifts to the position of the new peak appearing at 1). Our experience with various intents of growing mixed $MAPb(I,Br)_3$ thin films through the evaporation of MAI and $PbBr_2$ indicates that this growth route tends to form phase segregations with I-rich and Br-rich thin films co-existing instead of single phase films with mixed composition. In a variety of experiments we tried different substrate temperatures and $MAI/PbBr_2$ flux ratios, but were not able to find stable growth conditions that allow the deposition of single phase $MAPb(I,Br)_3$ perovskites with compositions in the middle of the compositional range following this growth route.

II. Co-evaporation of MABr and PbI_2

However, the situation is changed if the halides in the precursors are exchanged and MABr and PbI_2 are co-evaporated instead. With this precursor combination, we were able to grow single phase $MAPbI_{1-x}Br_x$ thin films with compositions x between 0.3 and 1 by co-evaporating MABr and PbI_2. Figure 5 b) shows the static growth of a single phase $MAPb(I_xBr_{1-x})_3$ thin film with a thickness of 780 nm, whose (200) position of 28.74° (2) corresponds to an x of approximately 0.3. This experiment demonstrates the potential to grow single phase $MAPbI_{1-x}Br_x$ thin films without initial phase segregation and under static growth conditions in vacuum. The film shows a nice homogenous morphology with crystallite sizes around 100-200 nm. A scanning electron micrograph of the film and more additional data on its photoluminescence can be found in the supporting information. From our preliminary experiments we conclude that by varying the $MABr/PbI_2$ flux ratios and substrate temperature, in principle all compositions between x= 0.3 and 1 should be accessible following this $MABr/PbI_2$ growth route.

Discussion

There is a heated debate on the intrinsic (in)stability of $MAPbI_3$, as its stability is a prerequisite for a successful application and commercialization as solar cell absorber. Several recent publications have predicted the thermodynamic instability of $MAPbI_3$ even at room temperature. Theoretical density functional theory (DFT) calculations resulted in a very small negative (-9.64 kj/mol)[46] or even positive (6.7 kJ/mol)[47] enthalpy for the formation for $MAPbI_3$ from its MAI and PbI_2 precursor constituents. Nagabushana et al. have suggested a positive enthalpy of formation of 34.50 kJ/mol for $MAPbI_3$ from their experimental solution calorimetry analysis.[23] In contrast to this, our results demonstrate the spontaneous formation of $MAPbI_3$ even at room temperature. By co-evaporating MAX and PbX_2 (X=I,Br,Cl) single phase perovskite films can be easily obtained. Dense films with good crystallinity giving intense XRD reflections could be formed without substrate heating, giving strong indication that the compound $MAPbI_3$ is energetically favourable and more stable than its two precursors phases, at least under the conditions used during the growth (high vacuum and MAX oversupply, 25°C). As an additional check, $MAPbI_3$ thin films did not show any variations when left inside the vacuum (no air exposure) inside our XRD setup for up to three days.

The before mentioned publications of Buin et al.[46] and Zhang et al.[47] predict an increasing thermodynamic stability of the $MAPbX_3$ perovskites in the sequence I-Br-Cl with the $MAPbCl_3$ being the most stable. As a matter of fact, the tolerance factor of $MAPbCl_3$ (table 1) is the closest to 1 and hence this compound is expected to come closest to the ideal cubic perovskite structure. For inorganic perovskites, the formation reaction becomes more exothermic with increasing tolerance factor.[48] From these considerations, one would expect $MAPbCl_3$ to be the most stable of the three perovskites.

In our experiments, all three single halide perovskites decompose in vacuum under loss of gaseous species into their corresponding lead halides. Interestingly, the first decrease of $MAPbX_3$ signal from the perovskite layers is observed at temperatures higher or similar to the evaporation temperatures used for the MAX temperatures: (MAI: 170°C/130°C, MABr: 230°C/130°, MACl: 110°C/110°C). In contrast to predictions, we found that $MAPbCl_3$ was the least thermally stable as it decomposed at the lowest temperatures with a very sharp transition. Already at 150°C, nearly all $MAPbCl_3$ was converted into its lead halide, while this only occurred at 260°C for the $MAPbI_3$ and $MAPbBr_3$, both showing much longer transitions. This is in agreement with experiments from Dualeh et al., who measured lower onset temperatures for the sublimation of MACl (185°C) than for MAI (234°C) in an thermogravimetric analysis of precursor powders.[9] In this work it was also suggested that decomposition of $MAPbI_3$ and $MAPbCl_3$ occurs via subsequent HX and methyl amine (CH_3NH_2) sublimation, and not in one single step of MAX sublimation. This is in agreement with recently published data on $MAPbX_3$ powders. Brunetti et al. also found the $MAPbCl_3$ compound to be significantly less stable than the Br/I counterparts under heating in non-ambient conditions.[49] Based on an additional Knudsen effusion mass spectroscopy and Knudsen effusion mass loss analysis, they proposed the following thermal decomposition pathway in non-ambient conditions:

$$MAPbX_3 \rightarrow PbX_2(s) + CH_3NH_2(g) + HX(g)$$

From their experiments, they calculated comparable decomposition enthalpies for $MAPbI_3$ and $MAPbBr_3$, but significantly lower ones for $MAPbCl_3$ for this specific decomposition route. The standard enthalpy of formation $\Delta H_f°(298K)$ from the elements for the $MAPbX_3$ compounds is

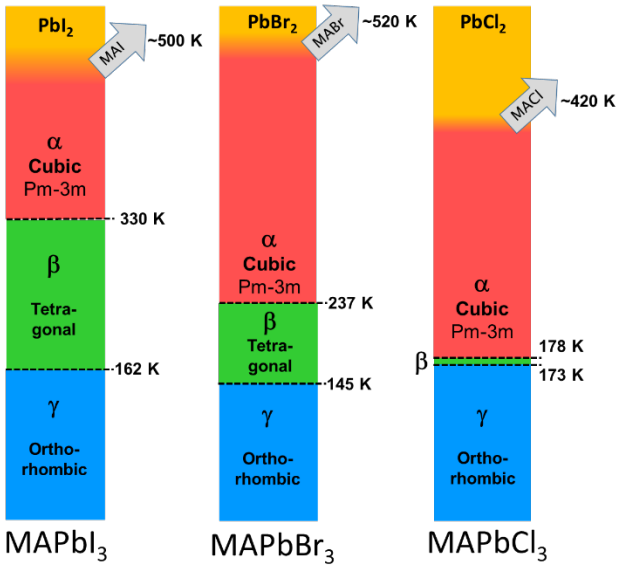

Figure 6: Schematic representation of the phase transitions and decomposition of $MAPbI_3$, $MAPbBr_3$ and $MAPbCl_3$.

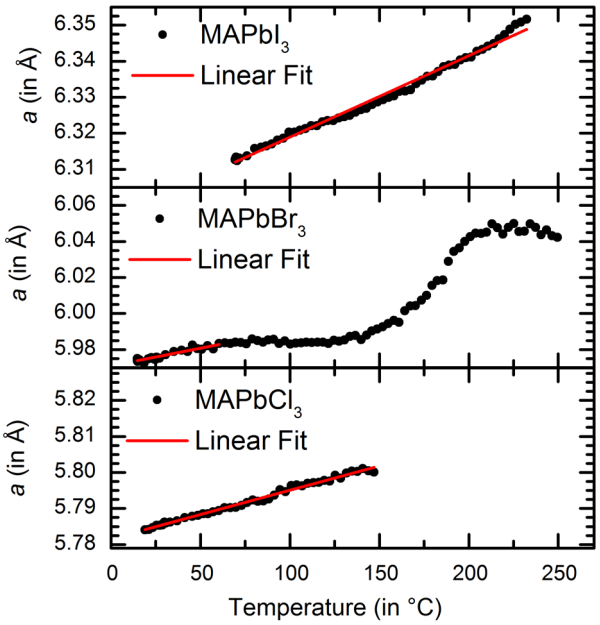

Figure 7: Temperature dependence of the lattice parameter *a* of the three $MAPbX_3$ perovskites studied in this work.

stated by Brunetti as -688.3 kJ/mol ($MAPbCl_3$), -567.5 kJ/mol ($MAPbBr_3$) and -403.6 kJ/mol ($MAPbI_3$). However, the decreasing trend of absolute values is mainly due to the trends observed for the formation of the corresponding lead halides and hydrogen halide species and therefore does not correspond to an increased stability of the $MAPbCl_3$ compound (table 2).[49]

Deretzis et al. have shown by in situ XRD measurements and ab initio calculations that $MAPBbI_3$ thin films should be thermodynamically relatively stable at room temperature and in the absence of water. Moisture (60% relative humidity) or thermal stress (150°C) reduced the lifetime of the perovskite material drastically.[50] Their DFT calculations supports the decomposition pathway postulated by Brunetti, as they show that calculated dissociation energies for varios atomic and molecular defects in $MAPbI_3$ are lowest for HI (1.31 eV). In other words, HI vacancies can be formed with little energetic cost. The volatile HI compound is expected to be readily lost, especially in vacuum conditions. In consequence, Deretzis et al. claim and observed an instability of the $MAPbI_3$ compound and degradation to PbI_2 already at room temperature if subjected to vacuum for prolonged times (1 month), due to dissociation processes at the surface and the loss of volatile HI species. It has to be noted, however, that their samples seem to have been in contact with air during sample preparation and therefore some moisture might have been already soaked into them.

In summary, there is still some debate on the gaseous species involved in the thermal decomposition[51, 52], but the degradation into PbX_2 is well established. The rate and onset of thermal decomposition is also discussed quite controversially and seem to strongly depend on a) air exposure b) temperature and c) deposition process.

We find $MAPbCl_3$ to be the least thermally stable of the three investigated $MAPbX_3$ compounds. As we cannot detect gaseous phases with our experimental setup, we could not verify the stated gaseous decomposition products or discriminate them from MAX. The phase transition temperatures (from literature) and the critical temperature T_c (from this work) are schematically depicted in figure 6.

Finally, from the 200 ($MAPbI_3$) and 100 ($MAPbBr_3$, $MAPbCl_3$) peak positions of our XRD data we can derive the temperature dependency of the lattice constants of the three cubic perovskite films (figure 7). The lattice parameter *a* of the cubic $MAPbI_3$ and $MAPbCl_3$ increase approximately linearly with temperature. From a linear fit to this data, the linear thermal coefficients of expansion at 70°C can be estimated as 3.6(1) x 10^{-5} K^{-1} for $MAPbI_3$. This compares well to the reported 4.4 x 10^{-5} K^{-1} based on powder diffraction and 4.2 x $10^{-5}K^{-1}$ based on first principle calculations in the quasiharmonic approximation.[53] For $MAPbBr_3$, the lattice parameter does not increase linearly in the temperature region where recrystallization and reorientation occurs (100-200°C). This impedes an accurate analysis of the thermal expansion coefficient in this range and might be caused by stress acting on the film during the recrystallization. We therefore limit the linear fit of the lattice parameter to the temperature range below 60 °C and calculate an α_L of 3.3(1) x $10^{-5}K^{-1}$ at room temperature. In the case of $MAPbCl_3$, we derive a linear coefficient of thermal expansion α_L of 2.3(1) x $10^{-5}K^{-1}$ at room temperature.

The opportunity to synthesize mixed perovskites with different halide ratios opens very attractive opportunities to tune the bandgap for specific applications. Despite the fact that it is the most investigated system, there is still a dispute if the $MAPbI_3$-$MAPbBr_3$ system is completely miscible or not. Several research groups have reported the synthesis of powders and thin films over the complete range of compositions.[54-56] Jacobsson et al. e.g. have prepared $MAPb(I_{1-x}Br_x)_3$ thin films by spin-coating covering the complete range of x from 1 to 0 and band gaps ranging from 1.59 eV to 2.31.[57] On the other hand, Brivio et al. have postulated on the basis DFT calculations that

at 300 K $MAPb(I_{1-x}Br_x)_3$ perovskites in the composition range between 0.3 <x< 0.6 should be thermodynamically unstable and should therefore segregate into I-rich and Br-rich phases.[44] Finally, Hoke et al. also found that mixed $MAPb(I_{1-x}Br_x)_3$ perovskites can be synthesized over the complete compositional range by spin-coating. For an increasing Br/I ratio they measured a linear decrease in the lattice parameter, but upon illumination a reversible phase segregation of I-rich and Br-rich phases occurred.[58] This phenomenon was later reproduced and verified by several research groups.[29, 59]

In our experiments, we found a continuous transition from $MAPbI_3$ to $MAPbBr_3$ under continuous supply of MABr. The transition from $MAPbBr_3$ to $MAPbI_3$, however possible, was not taken place in a continuous manner, but rather disruptive. Furthermore, we did not succeed to synthesize single phase $MAPb(I_{1-x}Br_x)_3$ thin films with x=0.3 from MAI and $PbBr_2$ precursors. To the contrary, in all our attempts phase segregation of different I-rich and Br-rich phases was observed. In contrast to this, evaporation of MABr and PbI_2 precursors lead to the growth of films with the desired stoichiometry without secondary phases even at room temperature.

We interpret these findings in view of the different Pb-X bonding strengths of I and Br and the different ionic radii. In both, the PbX_2 precursors as well as the final perovskite structure, the lead and halide ions build octaedra with similar bond length and bond strength. In view of the formation enthalpies of PbI_2/$PbBr_2$ or $MAPbI_3$/$MAPbBr_3$, it is energetically much easier to exchange one I by Br than the other way around (see table 2). Also from purely steric arguments the Br->I exchange is favoured before the I->Br exchange, as the smaller Br ion fit easily into the large Pb-I cage of $MAPbI_3$, while the large I ion does not fit in or move as easily within a smaller $MAPbBr_3$ lattice. In consequence, it is easier to substitute I by Br than Br by I. The more promising route towards the synthesis of mixed $MAPb(I,Br)_3$ thin films by co-evaporation is therefore by evaporating MABr precursors and co-evaporate it with PbI_2, or partly convert $MAPbI_2$ thin films by exposing them to MABr.

Table 3: Comparison of the critical temperature T_c and standard enthalpy of formation from the elements $\Delta H_f°$ for the perovskite compounds $MAPbX_3$ and the precursors. The critical temperature Tc at which approximately half of the perovskite film was decomposed into the lead halide was derived as outlined earlier in the manuscript.

X	I	Br	Cl	Ref.
T_c	~500 K	~520 K	~420 K	This work
$\Delta H_f°$ $MAPbX_3$ (kJ/mol)	-403.6	-567.5	-688.3	[49]
$\Delta H_f°$ PbX_2 (kJ/mol)	-175.5	-278.7	-359.4	[23]
$\Delta H_f°$ MAX (kJ/mol)	-200.7	-258.9	-298.3	[23]

Our results demonstrate on the one hand the power of *in situ* diagnostics, as we were able to conduct all measurements on pristinely grown thin films under vacuum conditions, i.e. without air exposure and directly during the growth. On the other hand, they verify the decomposition pathways and the thermal instability of $MAPbX_3$ thin films at moderate temperatures, and therefore underline worries on lifetime. The differences in the thermal decomposition rates reported by the different groups are a clear hint to the importance and influence of the different experimental conditions and the difficulty to obtain reliable and reproducible results for these hybrid perovskite compounds. In terms of mixed $MAPb(I,Br)_3$ thin films our results highlight the importance of the growth route and the selection of precursor combinations in order to grow single phase materials. They show how $MAPbIBr_2$ and similar compositions can be synthesized with simple two-source co-evaporation opening a promising perspective towards vacuum-based and low temperature fabrication of top cells for tandem applications.

Conclusions

In conclusion, we have demonstrated that single halide $MAPbX_3$ (X=I,Br,Cl) perovskite thin films with cubic crystal structure can be easily grown by co-evaporation of MAX and PbX_2 precursors. Upper limits for the thermal stability of these films before they decompose into the corresponding lead halides have been determined. Upon application of a linear temperature ramp of 3 K/min. approximately half of the perovskite film had been decomposed at a temperature of 230°C ($MAPbI_3$), 251°C ($MAPbBr_3$) and 148°C ($MAPbCl_3$). The linear increase of the lattice parameter based for $MAPbI_3$ and $MAPbCl_3$ allowed the determination of linear coefficient of thermal expansion α_L to $3.6 \times 10^{-5}K^{-1}$ ($MAPbI_3$), $3.3 \times 10^{-5}K^{-1}$ ($MAPbBr_3$) and $2.3 \times 10^{-5}K^{-1}$ ($MAPbCl_3$).

Furthermore, we could show that upon evaporation of MAI and $PbBr_2$, phase segregation takes place and two perovskite phases with stoichiometry close to $MAPbI_3$ and $MAPbBr_3$ tend to be present. Pure $MAPbBr_3$ can be converted into $MAPbI_3$ if it is heated to 120°C and exposed to MAI vapour, but the transition was not continuous but rather disruptive and not entirely complete. The analogous conversion of $MAPbI_3$ -> $MAPbBr_3$ took place continuously and completely. Single phase $MAPbI_2Br_1$ thin films were successfully synthesized by co-evaporating MABr and PbI_2 precursors. We thus were able to develop a new promising method for the preparation of mixed $MAPb(I,Br)_3$ thin films by a simple two-source co-evaporation approach.

Conflicts of interest

There are no conflicts to declare.

Acknowledgements

Financial support from the German Federal Ministry of Research and Education (BMBF) under contract number 03EK3570B (StrukturSolar II) is gratefully acknowledged.

References

1 A. Kojima, K. Teshima, Y. Shirai and T. Miyasaka, *Journal of the American Chemical Society*, 2009, **131**, 6050-6051.
2 H.-S. Kim, C.-R. Lee, J.-H. Im, K.-B. Lee, T. Moehl, A. Marchioro, S.-J. Moon, R. Humphry-Baker, J.-H. Yum, J. E. Moser and et al., *Sci. Rep.*, 2012, **2**, 591.
3 M. M. Lee, J. Teuscher, T. Miyasaka, T. N. Murakami and H. J. Snaith, *Science*, 2012, **338**, 643-647.
4 N. Arora, M. I. Dar, A. Hinderhofer, N. Pellet, F. Schreiber, S. M. Zakeeruddin and M. Grätzel, *Science*, 2017, **358**, 768-771.
5 W. S. Yang, J. H. Noh, N. J. Jeon, Y. C. Kim, S. Ryu, J. Seo and S. I. Seok, *Science*, 2015, **348**, 1234-1237.
6 Q. Dong, Y. Fang, Y. Shao, P. Mulligan, J. Qiu, L. Cao and J. Huang, *Science*, 2015, **347**, 967-970.
7 C. Wehrenfennig, G. E. Eperon, M. B. Johnston, H. J. Snaith and L. M. Herz, *Advanced Materials*, 2013, **26**, 1584-1589.
8 B. Conings, J. Drijkoningen, N. Gauquelin, A. Babayigit, J. D'Haen, L. D'Olieslaeger, A. Ethirajan, J. Verbeeck, J. Manca, E. Mosconi, F. D. Angelis and H.-G. Boyen, *Advanced Energy Materials*, 2015, **5**, 1500477.
9 A. Dualeh, P. Gao, S. I. Seok, M. K. Nazeeruddin and M. Grätzel, *Chemistry of Materials*, 2014, **26**, 6160-6164.
10 J. S. Manser, M. I. Saidaminov, J. A. Christians, O. M. Bakr and P. V. Kamat, *Acc. Chem. Res.*, 2016, **49**, 330-338.
11 N. Chander, A. F. Khan, P. S. Chandrasekhar, E. Thouti, S. K. Swami, V. Dutta and V. K. Komarala, *Appl. Phys. Lett.*, 2014, **105**, 033904-033904.
12 T. Leijtens, G. E. Eperon, S. Pathak, A. Abate, M. M. Lee and H. J. Snaith, *Nature Communications*, 2013, **4**, 2885-2885.
13 T. A. Berhe, W.-N. Su, C.-H. Chen, C.-J. Pan, J.-H. Cheng, H.-M. Chen, M.-C. Tsai, L.-Y. Chen, A. A. Dubale and B.-J. Hwang, *Energy Environ. Sci.*, 2016, **9**, 323-356.
14. T. Leijtens, K. Bush, R. Cheacharoen, R. Beal, A. Bowring and M. D. McGehee, *J. Mater. Chem. A*, 2017, **5**, 11483-11500.
15 C. Manspeaker, S. Venkatesan, A. Zakhidov and K. S. Martirosyan, *Current Opinion in Chemical Engineering*, 2017, **15**, 1-7.
16 O. Malinkiewicz, C. Roldán-Carmona, A. Soriano, E. Bandiello, L. Camacho, M. K. Nazeeruddin and H. J. Bolink, *Adv. Energy Mater.*, 2014, **4**, 1400345.
17 M. Sessolo, C. Momblona, L. Gil-Escrig and H. J. Bolink, *MRS Bulletin*, 2015, **40**, 660-666.
18 M. Liu, M. B. Johnston and H. J. Snaith, *Nature*, 2013, **501**, 395-398.
19 C. Momblona, O. Malinkiewicz, C. Roldán-Carmona, A. Soriano, L. Gil-Escrig, E. Bandiello, M. Scheepers, E. Edri and H. J. Bolink, *APL Materials*, 2014, **2**, 081504-081504.
20 G. Niu, X. Guo and L. Wang, *J. Mater. Chem. A*, 2015, **3**, 8970-8980.
21 S. Yang, W. Fu, Z. Zhang, H. Chen and C.-Z. Li, *J. Mater. Chem. A*, 2017, -.
22 T. Baikie, Y. Fang, J. M. Kadro, M. Schreyer, F. Wei, S. G. Mhaisalkar, M. Graetzel and T. J. White, *J. Mater. Chem. A*, 2013, **1**, 5628-5628.
23 G. P. Nagabhushana, R. Shivaramaiah and A. Navrotsky, *Proceedings of the National Academy of Sciences*, 2016, **113**, 7717-7721.
24 N. K. Kumawat, A. Dey, A. Kumar, S. P. Gopinathan, K. L. Narasimhan and D. Kabra, *ACS Applied Materials & Interfaces*, 2015, **7**, 13119-13124.
25 R. Comin, G. Walters, E. S. Thibau, O. Voznyy, Z.-H. Lu and E. H. Sargent, *Journal of Materials Chemistry C*, 2015, **3**, 8839-8843.
26 C. Li, J. Wei, M. Sato, H. Koike, Z.-Z. Xie, Y.-Q. Li, K. Kanai, S. Kera, N. Ueno and J.-X. Tang, *ACS Applied Materials & Interfaces*, 2016.
27 A. Sadhanala, S. Ahmad, B. Zhao, N. Giesbrecht, P. M. Pearce, F. Deschler, R. L. Z. Hoye, K. C. Gödel, T. Bein, P. Docampo, S. E. Dutton, M. F. L. De Volder and R. H. Friend, *Nano Letters*, 2015, **15**, 6095-6101.
28 P. Pistor, J. Borchert, W. Fränzel, R. Csuk and R. Scheer, *Journal of Physical Chemistry Letters*, 2014, **5**, 3308-3312.
29 E. L. Unger, L. Kegelmann, K. Suchan, D. Sörell, L. Korte and S. Albrecht, *J. Mater. Chem. A*, 2017, **5**, 11401-11409.
30 L. Gil-Escrig, A. Miquel-Sempere, M. Sessolo and H. J. Bolink, *The Journal of Physical Chemistry Letters*, 2015, **6**, 3743-3748.
31 V. M. Goldschmidt, *Die Naturwissenschaften*, 1926, **14**, 477-485.
32 G. Kieslich, S. Sun and A. K. Cheetham, *Chem. Sci.*, 2014, **5**, 4712-4715.
33 S. A. Bretschneider, J. Weickert, J. A. Dorman and L. Schmidt-Mende, *APL Materials*, 2014, **2**, 040701-040701.
34 C. Motta, F. El-Mellouhi, S. Kais, N. Tabet, F. Alharbi and S. Sanvito, *Nature Communications*, 2015, **6**, 7026-7026.
35 Y. Kawamura and H. Mashiyama, *Journal of the Korean Physical Society*, 1999, **35**, 1437-1437.
36 A. Poglitsch and D. Weber, *The Journal of Chemical Physics*, 1987, **87**, 6373-6373.
37 K.-H. Wang, L.-C. Li, M. Shellaiah and K. W. Sun, *Scientific Reports*, 2017, **7**.
38 R. D. Shannon, *Acta Crystallographica Section A*, 1976, **32**, 751-767.
39 J. Borchert, H. Boht, W. Fränzel, R. Csuk, R. Scheer and P. Pistor, *J. Mater. Chem. A*, 2015, **3**, 19842-19849.
40 G. Kaune, S. Hartnauer and R. Scheer, *physica status solidi (a)*, 2014, **211**, 1991-1996.
41 G. Li, J. Y.-L. Ho, M. Wong and H. S. Kwok, *The Journal of Physical Chemistry C*, 2015, **119**, 26883-26888.
42 I. C. Smith, M. D. Smith, A. Jaffe, Y. Lin and H. I. Karunadasa, *Chemistry of Materials*, 2017, **29**, 1868-1884.
43 D. Solis-Ibarra, I. C. Smith and H. I. Karunadasa, *Chem. Sci.*, 2015, **6**, 4054-4059.
44 F. Brivio, C. Caetano and A. Walsh, *The Journal of Physical Chemistry Letters*, 2016, **7**, 1083-1087.
45 L. Vegard, *Zeitschrift für Physik*, 1921, **5**, 17-26.
46 A. Buin, R. Comin, J. Xu, A. H. Ip and E. H. Sargent, *Chemistry of Materials*, 2015, **27**, 4405-4412.
47 Y.-Y. Zhang, S. Chen, P. Xu, H. Xiang, X. G. Gong, A. Walsh and S.-H. Wei, *Chinese Physics Letters*, 2018, **35**, 11-11.
48 A. Navrotsky, *ECS Transactions*, 2012, **45**, 11-17.
49 B. Brunetti, C. Cavallo, A. Ciccioli, G. Gigli and A. Latini, *Scientific Reports*, 2016, **6**.
50 I. Deretzis, A. Alberti, G. Pellegrino, E. Smecca, F. Giannazzo, N. Sakai, T. Miyasaka and A. La Magna, *Applied Physics Letters*, 2015, **106**, 131904-131904.
51 A. Latini, G. Gigli and A. Ciccioli, *Sustainable Energy & Fuels*, 2017, **1**, 1351-1357.
52 E. J. Juarez-Perez, Z. Hawash, S. R. Raga, L. K. Ono and Y. Qi, *Energy & Environmental Science*, 2016, **9**, 3406-3410.
53 F. Brivio, J. M. Frost, J. M. Skelton, A. J. Jackson, O. J. Weber, M. T. Weller, A. R. Goñi, A. M. A. Leguy, P. R. F. Barnes and A. Walsh, *Physical Review B*, 2015, **92**, 144308-144308.
54 P. Fedeli, F. Gazza, D. Calestani, P. Ferro, T. Besagni, A. Zappettini, G. Calestani, E. Marchi, P. Ceroni and R. Mosca, *The Journal of Physical Chemistry C*, 2015, **119**, 21304-21313.

55 J. H. Noh, S. H. Im, J. H. Heo, T. N. Mandal and S. I. Seok, *Nano Lett.*, 2013, **13**, 1764-1769.
56 B.-w. Park, B. Philippe, S. M. Jain, X. Zhang, T. Edvinsson, H. Rensmo, B. Zietz and G. Boschloo, *J. Mater. Chem. A*, 2015, **3**, 21760-21771.
57 T. J. Jacobsson, J.-P. Correa-Baena, M. Pazoki, M. Saliba, K. Schenk, M. Grätzel and A. Hagfeldt, *Energy & Environmental Science*, 2016, **9**, 1706-1724.
58 E. T. Hoke, D. J. Slotcavage, E. R. Dohner, A. R. Bowring, H. I. Karunadasa and M. D. McGehee, *Chem. Sci.*, 2015, **6**, 613-617.
59 C. M. Sutter-Fella, Y. Li, M. Amani, J. W. Ager, F. M. Toma, E. Yablonovitch, I. D. Sharp and A. Javey, *Nano Letters*, 2016, **16**, 800-806.